RESEARCH PAPER

Characterization and Photo-catalytic Efficiency of MnFe$_2$O$_4$/Zn$_2$SiO$_4$ for Aniline Degradation Using Box-Behnken Experimental Design and Simulated Solar Radiation

Zahra Sharifnezhad and Kazem Mahanpoor*

Department of Chemistry, Arak Branch, Islamic Azad University, Arak 086, Iran

ARTICLE INFO

ABSTRACT

In this research, Zn$_2$SiO$_4$ as a support and MnFe$_2$O$_4$ as a main photo-catalyst were individually synthesized and MnFe$_2$O$_4$ was fixed on Zn$_2$SiO$_4$ with solid state dispersion method. MnFe$_2$O$_4$ nano photo-catalyst was synthesized by co-precipitation method and reflux condition for 12 hours at 85°C in the presence of urea. For identification of catalysts Fourier-transform infrared (FTIR) spectroscopy, Field emission scanning electron microscopy (FESEM), Energy-dispersive X-ray spectroscopy (EDXS), transmission electron microscopy (TEM), X-ray diffraction (XRD), X-ray fluorescence (XRF) and Brunauer-Emmett-Teller (BET) techniques were used. The size of MnFe$_2$O$_4$ was determined about 15 nm after the fixation on the Zn$_2$SiO$_4$. The photo-catalytic efficiency of MnFe$_2$O$_4$/Zn$_2$SiO$_4$ was checked for degradation of aniline aqueous solution utilizing the irradiation of a 1 kW Xe lamp fitted with the AM1.5 filter (to simulate the solar light spectrum) in the presence of H$_2$O$_2$. Degradation process was modeled and optimized successfully applying response surface methodology (RSM) according to Box-Behnken designs. Experiment results were showed that initial concentration of aniline=5.5 ppm, H$_2$O$_2$ initial concentration=5.3 mM, pH=11 and nano photo-catalyst amount =0.4 g/L are optimal conditions and the degradation efficiency in this condition achieved is 96%. In the optimum conditions, arrangement of (MnFe$_2$O$_4$/Zn$_2$SiO$_4$)> (MnFe$_2$O$_4$)> (Zn$_2$SiO$_4$) was obtained for efficiency of photo-catalytic degradation of aniline in aqueous solution. Decomposition kinetic equation determined pseudo first order and k=0.0407.

How to cite this article

INTRODUCTION

Aniline, one of the aromatic organic compounds derived from material oil refining, is widely used in different industries to produce various materials such as polymer, oligomer, Isocyanides, agricultural pesticides, dyes and pigments [1]. This material has always brought about ecological problems of ground waters and surface waters. In addition, various toxic compounds are produced by aniline reaction to oxygen [2]. There are various methods such as physical treatment (adsorption on activated carbon, electro-dialysis and membrane), chemical treatment (chemical precipitation, photo-catalytic processes), biological for the purification of waters containing a mixture of organic and inorganic compounds [3]. Among these methods, the photo-

catalytic method is vital because of the complete removal of pollutants and their conversion to non-toxic materials such as CO$_2$, H$_2$O and N$_2$ through the advanced oxidation process (AOP) [4]. So far, many studies have been done to remove aniline by kind of photo-catalyst such as TiO$_2$, SnO$_2$, Cr/ZnO and CuO [5-12] (Summarized in Table 1) in which not only mineralization of aniline and intermediates have not happened completely (processes proved to require a lot of time) but also photo-catalyst isolation has been difficult.

In addition, the percentage of contamination is low and most importantly, photo-catalysts are not commercialized (Table 1). For example, ortho and para-aminophenol intermediates were formed in the process of aniline removal using titanium

* Corresponding Author Email: *k-mahanpoor@iau-arak.ac.ir*

Table 1. Summarized of many studies have been done to remove aniline by kind of photo-catalyst

Photo-catalyst	Synthesis method	Condition	%Removal
TiO_2	Commercial	*Aniline concentration: 100 mg dm^{-3}; Cat. amount: 25 %w/v; Particle size:30 nm; pH: 12; Temp.: ambient temperature; Removal time: 240 min; Particles surface area: 55 m^2 g^{-1}; Irradiation source: sunlight*	84.2
TiO_2	Commercial	*Aniline concentration: 0.04,0.05, 0.05 mmol l^{-1} (in different pH); Cat. Amount: 0.1 g l^{-1}; pH: 3, 7, 11; Temp.:25±2 °C; Removal time: 120 min; Particles surface area: 49.6 m^2 g^{-1}; Irradiation source: 20-W UV lamp (λ$_{max}$ 254 nm);*	38 (in pH=3), 79 (in pH=7), 96 (in pH=9),
TiO_2	sol–gel	*Aniline concentration: 0.047 mM; Catalyst amount: 1 g l^{-1}; Particle size: 37.0 μm; pH: 7; Temp.: 30 ± 0.5 °C; Removal time: 240 min; Particles surface area :139.6 m^2 g^{-1}; Irradiation source: 3-W light emitting diode (visible light: 400 to 700 nm)*	72
Cr:ZnO	hydro-thermal	*Aniline concentration: 150, 200, 250 mg l^{-1}; Catalyst amount: -; Particle size: 60-160 nm ; pH: 9; Removal time: 360 min; Irradiation source: sunlight*	93
CuO		*Aniline concentration: 50 mg l^{-1}; Catalyst amount:0.1 g l^{-1}; Particle size: >50 nm; pH: 7; Temp.: 27±3 °C; Removal time: 90 min; Irradiation source: UV-C*	89
SnO_2	hydrothermal	*Aniline concentration: 20 mg l^{-1}; Particle size :120-280 nm diameter & 300 nm length; pH: 10; Temp.: room temperature; Removal time: 120 min; Particles surface area: 88 m^2 g^{-1}; Irradiation source: 8W UV-A;*	96
TiO_2	Commercial	*Aniline concentration: 3*10^{-3} mg dm^{-3}; pH: 10.8; Temp.: ambient temperature; Removal time: 360 min; Irradiation source: 200W Mercury Xenon*	complete degradation
TiO_2, MWCNT*, TiO2: MWCNT 80:20 (w/w)	sol-gel, commercial, sol-gel & hydration-dehydration technique	*Aniline concentration: 1 mM; Catalyst amount:125, 250 mg ml^{-1}; Removal time: 180 min; Particles surface area: 80,50 and 100 m^2 g^{-1}; Irradiation source: mercury vapor lamp with filter (λ$_{max}$: 366, 436 & 546 nm); inlet O$_3$ concentration:50 g m^{-3}, gas flow rate: 150 cm^3 min^{-1}*	88, 85, 90

* MWCNT: Multi-walled carbon nanotubes

dioxide in the pH=12 and 84.2 percent of aniline is converted to H_2O and CO_2 after 240 minutes [5].

Poly-functional oxide nanoparticles such as ABO_3 and AB_2O_4 spinel seem to have magnetic and photo-catalytic properties. Spinel ferrites, AFe_2O_4 (A=Mn, Mg, Zn, Co, Fe etc.) have exclusive features and functionality to remove various contaminants from water and wastewater (Das, 13). Among the spinel ferrites, manganese ferrite spinel was chosen as a main catalyst because it has narrow band-gap and multiple oxidation states [14]. In addition, its initial raw materials are abundant, inexpensive and available. The researches have shown that these compound preparation methods are diverse [15,16].

These methods are not applicable due to the complexity of the preparation process, high cost, high consumption time, high reaction temperature, environmental constituents and environmental problems. On the other hand, properties and performance of the catalyst are influenced by the raw materials and the manufacturing process. Due to these problems, $MnFe_2O_4$ was synthesized using co-precipitation method to produce nano particles (NPs), to reduce cost, to increase the degradation rate, to create maximum efficiency and minimum ecological problems. To prevent the ecological impact on NPs and to facilitate their collection to reuse catalyst, utilizing magnetic spinels ($MnFe_2O_4$) became the primary focus of the research [13,15]. The separation of the catalyst from water is an inevitable problem. Stabilizing the catalysts on the base, in addition to increasing the active surface and facilitating the separation of the catalyst from the water, improves their stability. In this research, Zn_2SiO_4 was used a catalyst base because of it has chemical and thermal stability, insolubility in water and proper surface properties [13,15,17]. Therefore, $MnFe_2O_4/Zn_2SiO_4$ was synthesized as a new and effective photo-catalyst. EDXS, XRD,

XRF, FESEM, BET and FTIR techniques were used to identify synthesized particles. The processes of aniline degradation in the presence of MnFe$_2$O$_4$ / Zn$_2$SiO$_4$ and the simulation of sunlight (a 1 kW Xe lamp fitted with an AM1.5 filter) was used to obtain the catalyst performance.

With stabilizing MnFe$_2$O$_4$ on Zn$_2$SiO$_4$ (as a new base) was produced unique catalyst (MnFe$_2$O$_4$/ Zn$_2$SiO$_4$) for aniline degradation.

Although MnFe$_2$O$_4$ has been used to remove many pollutants in photocatalytic process, MnFe$_2$O$_4$ and MnFe$_2$O$_4$/Zn$_2$SiO$_4$ has not been reported to remove aniline. This is exactly the novelty of this study.

Degradation processes were modeled, and affective factors such as aniline initial concentration, H$_2$O$_2$ initial concentration, pH and the amount of nano photo-catalyst were optimized successfully applying RSM according to Box-Behnken design [18]. The kinetics of aniline photo-degradation reactions to presence of MnFe$_2$O$_4$/ Zn$_2$SiO$_4$, MnFe$_2$O$_4$ and Zn$_2$SiO$_4$ were investigated under optimum condition and their photo-catalytic efficiency were compared. Repeatability of the MnFe$_2$O$_4$/Zn$_2$SiO$_4$ efficiency was demonstrated by performing the aniline degradation test five times under optimum condition using depreciated photo-catalyst.

EXPERMENTAL

Materials and Apparatus

Chemical reagents include zinc sulfate (ZnSO$_4$.7H$_2$O), manganese nitrate (Mn(NO$_3$)$_2$.4H$_2$O), iron nitrate (Fe(NO$_3$)$_3$.9H$_2$O), NaOH, urea, aniline and silicon dioxide (SiO$_2$=99.5%w/w, 10-20 nm particle size (BET)) were purchased from Sigma Aldrich Company. Other materials such as ethanol, hydrogen peroxide (35% w/w) were taken from Merck Company.

The Infrared spectra of all materials were taken with Fourier transform infrared spectroscopy (Spectrum Two FT-IR Spectrometer, Perkin-Elmer). XRD analysis of the samples was done applying an X-ray spectrometerX27-mini diffract-meter. XRF and BET analysis of MnFe$_2$O$_4$/Zn$_2$SiO$_4$ were done utilizing X-ray fluorescence ARL PER FORM'X and BELSORP-mini II, Bell Japan, respectively. The morphology, elemental mapping of the samples and the particles size were determined employing Field emission scanning electron microscopy (FESEM, XL-30, Philips) and transmission electron microscopy (TEM, Zeiss-EM10C-100 KV, Germany).

Energy Dispersive X-ray Spectroscopy (EDXS, Philips) was used to determine the type and the percentage of elements. The UV-Vis spectra of the aniline in aqueous media were recorded by Agilent 8453 UV-visible spectrophotometer. The photo-catalytic decomposition of aniline was performed in the one-liter batch photo-reactor and 1 kW Xe lamp fitted with AM1.5 filter (to simulate the solar light spectrum).

Preparation of Zn$_2$SiO$_4$, MnFe$_2$O$_4$ and MnFe$_2$O$_4$/ Zn$_2$SiO$_4$

To prepare Zn$_2$SiO$_4$ NPs in correspondence with documents [17], 0.1 mole of [ZnSO$_4$.7H$_2$O] was completely dissolved in 100 ml distilled water. Then, 100 ml NaOH, 0.2 moles were added drop by drop to zinc sulfate solution and stirred at 80 °C. The solution was cooled to ambient temperature. Precipitated Zn(OH)$_2$ was separated from the solution by centrifuge, it washed with distilled water and it dried at 100 °C for 12 h.

0.2 mole Zn(OH)$_2$ and 0.1 mole silica powder with high purity were added to 200 ml distilled water and this mixture was stirred for 4 h at 80 °C. Precipitate was centrifuged and dried at 80 °C in oven and finally calcined at 1050 °C.

Based on previous research, MnFe$_2$O$_4$ NPs were synthesized in the urea aqueous solution to the reflux condition. To do this, 0.2 mole of (Fe(NO$_3$)$_3$.9H$_2$O) and 0.1 mole of (Mn(NO$_3$)$_2$.4H$_2$O) were dissolved in 200 ml water and 250 ml of 0.4 molar urea was added to this solution. This solution was heated on the water bath at 85°C for 12 h in the reflux condition. Precipitate was separated by centrifuge and washed with water and ethanol (respectively) several times. It was dried at 80°C in oven and calcined at 990 °C [19,20].

To prepare MnFe$_2$O$_4$/Zn$_2$SiO$_4$, MnFe$_2$O$_4$ nanoparticles were mechanically mixed with Zn$_2$SiO$_4$ (1:3 w/w %) in the presence of ethanol by agate pestle and mortar. This homogeneous mixture was dried at 110 °C in oven for 2 h and calcined at 1050 °C in the furnace for 5 h. Precipitate was sieved employing 100 mesh standard sieves.

Design of Experiment (DOE)

Design of experiment by Box-Behnken method has been used to obtain the minimum test required to obtain the effect of variables and relationship between variables on the percentage of aniline degradation also it used for optimization and mathematical modeling [19].

Table 2. Level of factors

Variable (Operation factor)	Factors	Level		
	Uncoded	-1	0	+1
Aniline conc. (ppm)	x_1	1	5.5	10
pH	x_2	5	8	11
Initial H_2O_2 conc. (mM)	x_3	1.76	3.53	5.3
Nano photo-catalyst amount (g L^{-1})	x_4	0.2	0.4	0.6

Table 3. Coded and uncoded Box-Behnken design matrix along with experimental and predicted response

Run	Coded variables				Uncoded variables				Response (Aniline degradation %)	
	X_1	X_2	X_3	X_4	x_1	x_2	x_3	x_4	Experimental	Predicted
1	-1	0	-1	0	1	8	1.76	0.4	87.00	86.22
2	0	-1	-1	0	5.5	5	1.76	0.4	94.00	95.20
3	1	0	-1	0	10	8	1.76	0.4	83.00	82.78
4	0	1	-1	0	5.5	11	1.76	0.4	91.64	91.90
5	1	-1	0	0	10	5	3.53	0.4	90.02	90.70
6	-1	0	0	-1	1	8	3.53	0.2	82.00	83.45
7	-1	0	0	1	1	8	3.53	0.6	75.03	75.97
8	0	0	1	1	5.5	8	5.3	0.6	81.21	82.15
9	1	0	1	0	10	8	5.3	0.4	87.36	86.94
10	0	0	1	-1	5.5	8	5.3	0.2	82.95	84.16
11	0	0	0	0	5.5	8	3.53	0.4	85.10	85.37
12	0	1	0	1	5.5	11	3.53	0.6	95.04	95.40
13	0	-1	1	0	5.5	5	5.3	0.4	83.25	83.22
14	1	0	0	1	10	8	3.53	0.6	90.75	90.00
15	-1	-1	0	0	1	5	3.53	0.4	82.00	81.55
16	0	1	0	-1	5.5	11	3.53	0.2	91.94	91.53
17	0	0	0	0	5.5	8	3.53	0.4	86.59	85.37
18	-1	0	1	0	1	8	5.3	0.4	74.18	73.20
19	-1	1	0	0	1	11	3.53	0.4	90.00	89.80
20	0	0	-1	-1	5.5	8	1.76	0.2	85.40	85.18
21	1	1	0	0	10	8	3.53	0.4	90.01	90.96
22	1	0	0	-1	10	8	3.53	0.2	80.00	79.73
23	0	-1	0	1	5.5	5	3.53	0.6	89.02	88.67
24	0	-1	0	-1	5.5	5	3.53	0.2	90.83	89.74
25	0	0	-1	1	5.5	8	1.76	0.6	90.48	89.99
26	0	0	0	0	5.5	8	3.53	0.4	84.87	85.37
27	0	1	1	0	5.5	11	5.3	0.4	96.00	95.03

According to Box-Behnken design (using a randomized method) with four variables and three levels for each variable, 27 tests were determined.

Variable levels were determined corresponding to Table 2.

The Minitab 17 statistical software was used to design the Box-Behnken. Experimental conditions were performed based on the design matrix (Table 3). The pH of solutions was modified by NaOH and H_2SO_4 (0.01 M). All of the experiments were performed with 1 liter of aqueous solutions to the batch reactor with stirring at ambient temperature. In each operation, photo-catalysts were added to aqueous solutions and maintained in the dark space for 30 minutes before irradiation. Then H_2O_2 with specific concentration was added to solution and maintained under simulated solar light irradiation (1 kW Xe lamp fitted with AM1.5 filter) for 120 minutes. The absorbance of aniline solutions before and through irradiation was analyzed applying UV-Vis spectrophotometer at 230 nm, within 120 minutes at 10-minute intervals. The percentage of aniline degradation was calculated by the equation (1) for 27 experiments separately.
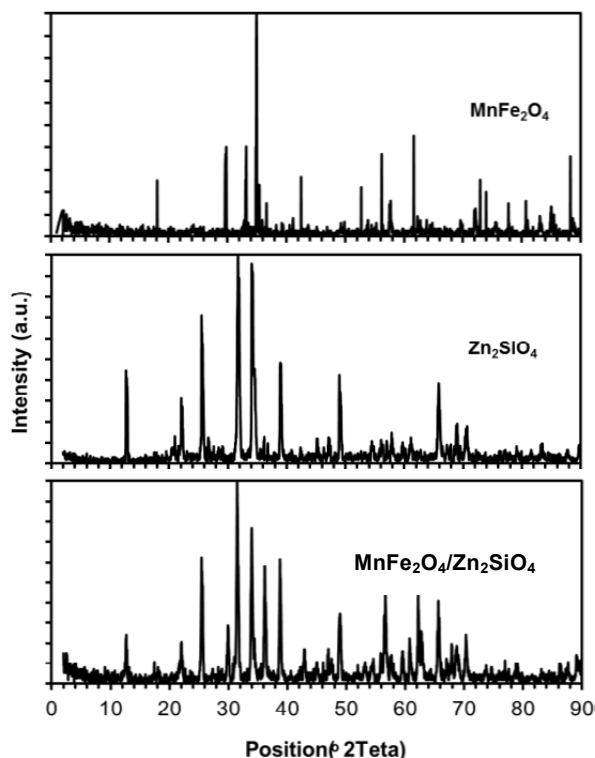
Fig. 1. XRD patterns of MnFe₂O₄, Zn₂SiO₄ and MnFe₂O₄/Zn₂SiO₄ NPs

$$Deg.\% = \frac{A_o - A_t}{A_0} \times 100 \qquad (1)$$

Where A_0 is absorption amounts to maximum absorption wavelength (230 nm) at t=0 (before irradiation), A_t is absorption amounts to at maximum absorption wavelength after t minute irradiation.

The most important parameters such as probability values (P-values), standard deviation of the residuals (S), R^2, adjusted R^2 and predicted R^2 values were determined by variance analysis (ANOVA). The adequacy of the model was checked by residual plots of degradation. Then, response optimizer was applied to recognize the best operating conditions or global solutions to optimize the aniline degradation, to decrease costs, to increase sensitivity of factors and desirability.

In the optimum condition, photo-catalytic efficiency and kinetic of MnFe₂O₄/Zn₂SiO₄, MnFe₂O₄ and Zn₂SiO₄ were compared.

The catalyst performance was also studied after five times the experiment in optimal conditions.

RESULTS AND DISCUSSION
Characterization of MnFe₂O₄/Zn₂SiO₄ photo-catalyst
X-Ray Diffraction and X-ray Fluorescence analysis

The XRD patterns of the synthesized samples (MnFe₂O₄, Zn₂SiO₄ and MnFe₂O₄/Zn₂SiO₄) were taken as follows (Fig. 1).

The comparison of these diffraction patterns with the results taken by other researchers confirmed the synthesis of MnFe₂O₄/Zn₂SiO₄ [19, 21-24]. The average size of MnFe₂O₄ supported on Zn₂SiO₄ based on the collected data from XRD and the use of Debye-Scherrer equation [23] was obtained about 19.1nm.

XRD sharp and intense peaks within diffraction patterns of synthetic materials demonstrated that there is a high degree of crystallinity in all synthetic NPs. Also, MnFe₂O₄ stabilization on Zn₂SiO₄ is proved by comparison of diffraction pattern of MnFe₂O₄/Zn₂SiO₄ with those of MnFe₂O₄ and Zn₂SiO₄. The presence of Zn₂SiO₄ and MnFe₂O₄ peaks in XRD patterns of MnFe₂O₄/Zn₂SiO₄ indicate that the crystalline structure of these materials is not altered in the catalyst.

Furthermore, elemental and oxide compositions of MnFe₂O₄/Zn₂SiO₄, which are shown in Table 4, were determined by XRF. These results demonstrate that atomic ratios are proportional to MnFe₂O₄/Zn₂SiO₄ structure.

Fourier transforms infrared spectroscopy

FTIR spectra of $MnFe_2O_4/Zn_2SiO_4$, $MnFe_2O_4$ and Zn_2SiO_4 are displayed in Fig. 2 and all the absorption bands and their assignment for $MnFe_2O_4/Zn_2SiO_4$ are summarized in Table 5. The observing index peaks of $MnFe_2O_4$ and Zn_2SiO_4 in $MnFe_2O_4/Zn_2SiO_4$ spectrum, confirm synthesis of $MnFe_2O_4/Zn_2SiO_4$ nanoparticles.

The peaks at 578 and 460 cm^{-1} in spectrum correspond respectively to deformation vibrations of Fe-O and Mn-O in tetrahedral and octahedral coordination compounds in the spinel structure. Moreover, 1630 and 3435 cm^{-1} bands are related to O-H bending and stretching vibration, a fact which indicates water and the absorbed OH at the catalyst surface [25-27]. Also, position of 3436 and 1630 cm^{-1} bands are correlated with bonding and stretching vibrations of O-H in Si-OH [22,23]. The 1150 cm^{-1} bond is related to Mn-O-H bending vibration. The 978, 933 and 902 cm^{-1} bonds correspond to asymmetric stretching vibrations and 870 cm^{-1} peak is related to symmetric stretching vibrations of Si-O in SiO_4 units. Symmetric and asymmetric stretching vibrations of ZnO in ZnO_4 units appear at 578 and 616 cm^{-1}, respectively [23,24]. The results of FTIR analysis demonstrate that there is not any impurity in the crystal lattice and also it exhibits that the calcinations temperature for preparation of $MnFe_2O_4/Zn_2SiO_4$ is suitable.

FESEM, EDXS and TEM analysis

The morphology of $MnFe_2O_4/Zn_2SiO_4$, (Figs. 3(a-c)) was obtained by FESEM. The exact investigation of the magnified pictures (Figs. 3(b) and (3c)) reveals the agglomeration of NPs. Considering that the formation and growth of these NPs are based on the reaction of urea, manganese nitrate and iron nitrate precursors under hydrolysis and reflux condensation in water (based on reactions (2-6)), probably, the agglomeration of NPs and the formation of dense grains are due to solvent polarity and high calcination temperature.

To acquire more information, the analysis of Energy Dispersive X-ray spectroscopy (EDXS) of $MnFe_2O_4/Zn_2SiO_4$ was taken. Fig. 3(d) indicates the EDXS spectra and the elemental composition of $MnFe_2O_4/Zn_2SiO_4$. The EDXS analysis of $MnFe_2O_4/Zn_2SiO_4$ spectrum reveals the presence of Fe, Mn, Zn, Si and O elements.

Fig. 4 (a, b) shows the morphology and core-shell structure of $MnFe_2O_4/Zn_2SiO_4$. Magnified images to demonstrate that $MnFe_2O_4$ shell with a thickness of less than 15 nm formed into the Zn_2SiO_4 core.
Elemental mapping of iron, manganese, zinc, silica and oxygen in $MnFe_2O_4/Zn_2SiO_4$ are shown in Fig. 5(b-f) by green, orange, red, blue and yellow points, respectively. Spatial distribution, compositional zonation and the presence of the elements in $MnFe_2O_4/Zn_2SiO_4$ is characterized by these colored points.

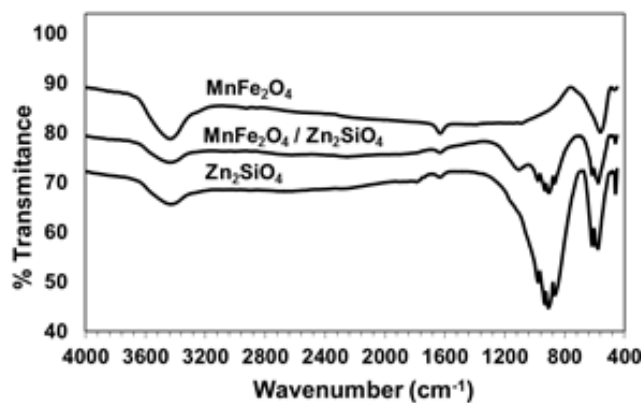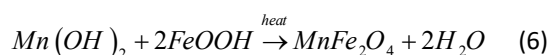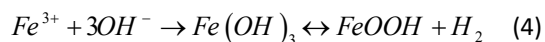$$\left(NH_2\right)_2 CO + H_2O \rightarrow 2NH_3 + CO_2 \qquad (2)$$

$$NH_3 + H_2O \rightarrow NH_4^+ + OH^- \qquad (3)$$

$$Fe^{3+} + 3OH^- \rightarrow Fe\left(OH\right)_3 \leftrightarrow FeOOH + H_2 \quad (4)$$

$$Mn^{2+} + 2OH^- \rightarrow Mn\left(OH\right)_2 \qquad (5)$$

$$Mn\left(OH\right)_2 + 2FeOOH \xrightarrow{heat} MnFe_2O_4 + 2H_2O \quad (6)$$
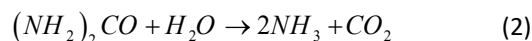
Fig. 2. FTIR spectra of $MnFe_2O_4$, $MnFe_2O_4/Zn_2SiO_4$ and Zn_2SiO_4

Table 4. XRF results for MnFe$_4$O$_4$/Zn$_2$SiO$_4$

Oxid	Weight%	Element	Weight%
MnO	6.61	Mn	5.12
Fe$_2$O$_3$	28.94	Fe	10.12
SiO$_2$	17.33	Si	8.1
ZnO	46.74	Zn	37.55
Al$_2$O$_3$	0.08	Al	0.02
K$_2$O	0.02	K	0.01
CaO	0.02	Ca	0.012
MgO	0.03	Mg	0.02
L.O.I	0.23	L.O.I	0.23

Table 5. FTIR Wavenumber and band assignment for Mn-Fe$_2$O$_4$/Zn$_2$SiO$_4$

Wavenumber (cm^{-1})	Assignment
3435	O-H stretching vibration in H$_2$O O-H stretching vibration in Si-OH
1630	O-H bending vibration in H$_2$O O-H bending vibration in Si-OH
1150	Mn-O-H bending vibration
978,933,902	Si-O asymmetric stretching vibration
870	Si-O symmetric stretching vibration in SiO$_4$ units, Fe-O-H bending vibration
697	Fe-O and Mn-O stretching vibration
616	Zn-O asymmetric stretching vibration in ZnO$_4$ units, Fe-O vibration in FeOOH
578	Zn-O symmetric stretching vibration in ZnO$_4$ units, Si-O bending vibration, Fe-O deformation vibration
460	Si-O asymmetric deformation vibration in SiO$_4$ units, Si-O symmetric stretching vibration in SiO$_4$ units, Mn-O deformation vibration

BET analysis

BET analysis for synthesized MnFe$_2$O$_4$/Zn$_2$SiO$_4$ was performed by determining the amount of adsorption and desorption of N$_2$ gas at 77 K (Fig. 6). Amount of "means pores area" and "means pores volume" were determined about 52.79 m^2 g^{-1} and 0.058 cm^3 g^{-1} respectively. These amounts indicate the notable physical interaction of N$_2$ gas with the surface of NPs molecules. Fig. 6 (a) shows that the isotherm structure is similar to that of the IV type isotherm. Also, hysteresis displays the existence of meso pores with cylindrical structure of NPs (Fig. 6(a)) [28]. Pore size distribution was found by Barclay James Harvest (BJH) plot (Fig. 6(c)). As the results present, the mean pore diameter is about 4.43 nm.

Modeling using a Box-Behnken design with RSM Analysis of variance (ANOVA) and model fitting

The RSM was used to understand and optimize important factors, to determine and refine the model [18]. The Box-Behnken design, one of response surface design (RSD) was used because this method needs fewer tests and all the factors are not placed simultaneously at a high or low level and the coefficients are estimated to be the second order. Also, the Box-Behnken design, as compared to other methods, reduces the number of tests without reducing accuracy [18]. According to Box-Behnken design with four factors and three levels, cases such as experimental conditions, factor combinations and run-order of 27 experiments were determined by randomizing corresponding to Table 3 [18].

In the photo-catalytic process, the semiconductor of MnFe$_2$O$_4$/Zn$_2$SiO$_4$ was used as main catalyst along with simulated radiation of the solar light on the photo-catalyst surface. In order to determine the efficiency of the photo-catalyst, aniline degradation process (27 experiments)

was performed corresponding to design matrix (Table 3). In photo-catalytic degradation process, corresponding to Fig. 7, light radiation takes effect on the surface of the semiconductor and electrons are transferred from the valence band to the conductive band. Therefore, the holes in the valence bands and the electrons in conducting layer are created. Holes are strongly oxidizer. Thus, hydroxyl ion from NaOH and H$_2$O molecules reacts with photo-catalyst valance bond holes. These steps redound to the formation of hydroxyl radicals. Electrons in the valence band react with dissolved oxygen, and consequently superoxide radicals are produced. Then superoxide radicals after some steps are converted to hydroxyl radicals. Superoxide and hydroxyl radicals are very reactive. Hydrogen peroxide can increase the production of radicals. Also, the formation of hydroxyl radicals is increased by the change of pH and catalyst. Accordingly, aniline is degraded and converted to CO$_2$ and H$_2$O by active radicals after some steps. As a consequence, percentages of aniline degradation for 27 experiments are affected by type, level and combination of factors.

After calculating the percentage of aniline degradation by equation 1 (for 27 experiments) and performing an analysis of Box-Behnken design, analysis of variance (ANOVA) was investigated. Studying the amounts of P-values in the ANOVA table for any variable (section a, Table 6) shows that the impact on second order factors of x4x4 and x3x3 is insignificant because they have P-values>0.05. In this research, confidence level
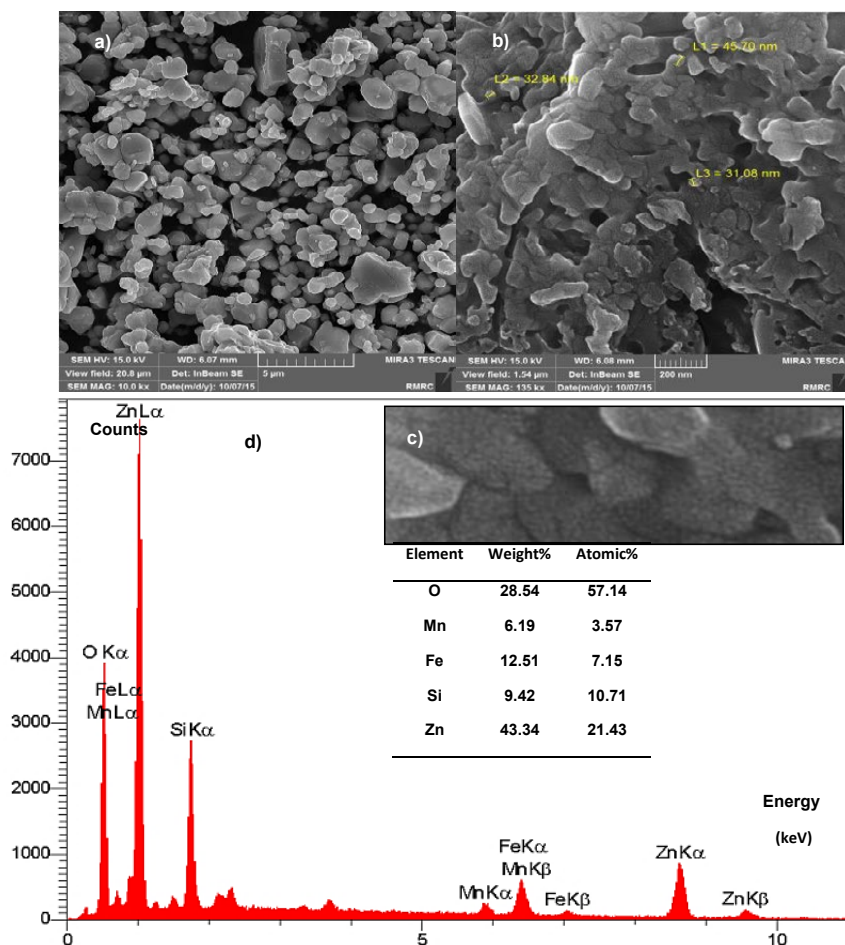
Element	Weight%	Atomic%
O	28.54	57.14
Mn	6.19	3.57
Fe	12.51	7.15
Si	9.42	10.71
Zn	43.34	21.43

Fig. 3. (a, b and c) FESEM images of $MnFe_2O_4/Zn_2SiO_4$, (d) EDXS elemental composition of $MnFe_2O_4/Zn_2SiO_4$

has been chosen equal to α=0.05. Therefore, the effects that have P-values>0.05 are insignificant and vice versa, So second order terms with large P-values were omitted and the analysis response surface design was once again repeated and the result of ANOVA was recorded in section b of Table 6. In the models listed in Table 7, comparing P-values of lack of fits (after removing insignificant terms) appraises the fit of the model. According to Table 7, the P-values of the full quadratic model are more than 0.05; thus, this model accurately fits the data. Since the amounts of P-values are less or equal to 0.05 in other models, they couldn't cover the data properly. The statistical parameters such as adjusted R^2 and standard deviation of the residuals in full quadratic model prove the suitability of full quadric model in fitting the data of response surface (compared to the other models). On the other hand, the amounts of P-values for interaction factors (x_1x_2, x_1x_3, x_1x_4, x_2x_3,

x_2x_4 and x_3x_4) and second order term (x_1x_1, x_2x_2) to express the curvature of response surface.

The R^2 value points out that the predictors (factors) illustrate 98.06% of the variance in aniline degradation yield. The adjusted R^2 is 96.40%, a fact which explains the number of effects on the model. Both value to indicate that the model is well suited to the data. The amount of the predicted R^2 is 92.08%. There are no over fit values of the model, so it has sufficient predictive power.

The standard deviation of the residual in final regression is equal to 1.05677. This shows that actual data have a 1.05677 standard distance from the regression line or the predicted value. Also, small amount of S indicates that the model is suitably enough.

Model modification, adequacy checking and optimization

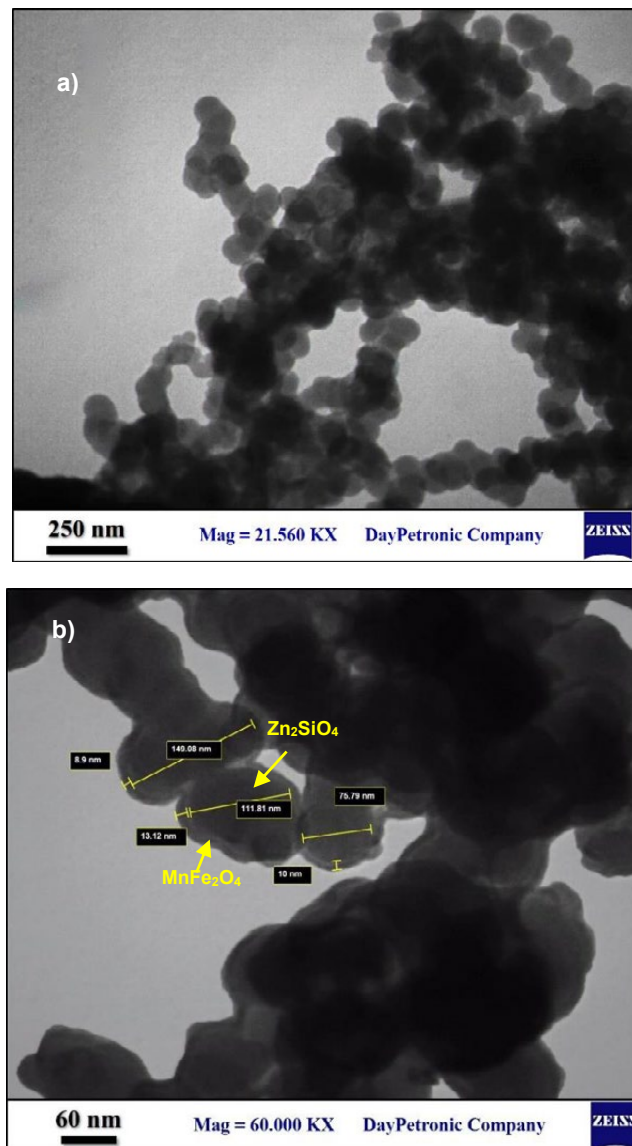After determining the significant and insignificant

Fig. 4. (a, b) TEM images of MnFe$_2$O$_4$/Zn$_2$SiO$_4$

effects, insignificant factors including x4x4 and x3x3 were removed in order to improve the model. The estimated regression coefficients for the degradation of aniline were acquired by equation (7-8) based on un-coding data. Where Y is aniline degradation yields (response), x_i and x_j are factors, β_0 is overall mean, β_i and β_{ij} are regression coefficients and ε is random error with normal distribution (mean = 0 and standard distribution of δ).

Omitting insignificant factors, R^2 lowered slightly (from 98.10% to 98.06%) and the amount of adjusted R^2, which is more important, increased a little (from 95.89% to 96.40%). The predicted

R^2, which is an important parameter in predicting response from new observations, changed from 89.83% to 92.08%. The model with bigger value of predicted R^2 has larger predictive ability for new observations. Also, the reduction of the sum of squares of the prediction error (PRESS) from 82.128 to 63.969 through removing the insignificant factors indicates greater predictive ability of the model, too.

The equation (8) indicates that aniline concentration and pH have second order effects, whereas initial concentration of H$_2$O$_2$ and the amount of MnFe$_2$O$_4$/Zn$_2$SiO$_4$ photo-catalyst have just linear effects.
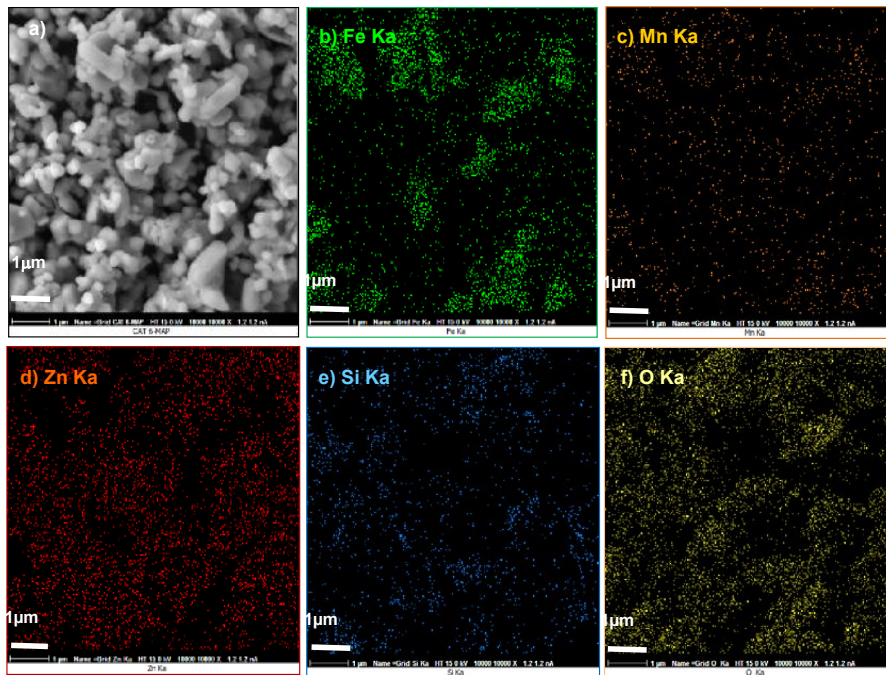
Fig. 5. (a-f) Elemental mapping of $MnFe_2O_4/Zn_2SiO_4$: (a) SEM image, (b) Fe, (c) Mn, (d) Zn, (e) Si and (f) O distribution
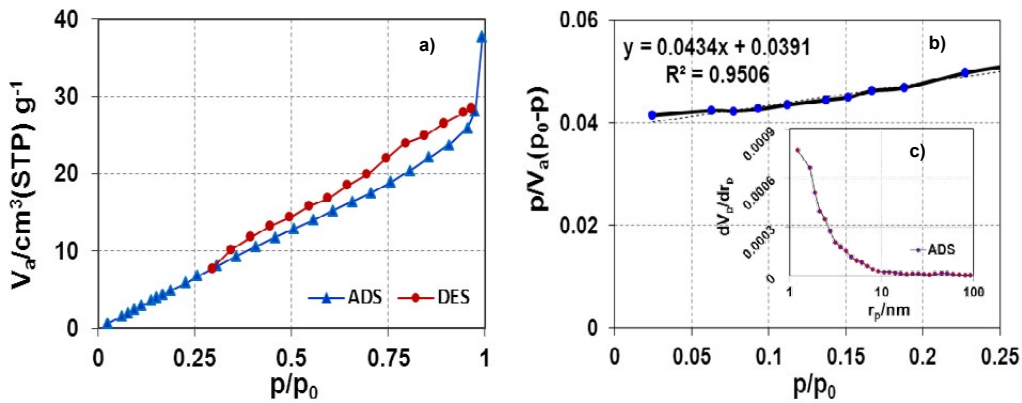

Fig. 6. (a) N_2 Adsorption and desorption isotherm, (b) N_2 adsorption isotherm, (c) BJH plot (pore size distribution) for $MnFe_2O_4/Zn_2SiO_4$

The distribution and the independence of the residuals were studied to check the adequacy of the model (Fig. 8). The residuals, which are the difference between the test response and the predicted response, are normal if the points are near the regression line (Fig. 8(a)). Regarding that the residuals against fitted values in Fig. 8(b) are completely random and scattered; therefor, residuals are independent. This means that the residuals have non-constant variance.

Fig. 8(c) exhibits a histogram of the residuals. It indicates that the errors are random and there are no data collection orders for residuals. Structure of Fig. 8(d) approves that residuals do not have correlation with each other. Thus, all of the mentioned interpretations confirm that ANOVA table (Table 6) is reliable and the model can predict aniline degradation yields ± 1.05677 with a 95% confidence level (confidence interval).

$$Y = \beta_0 + \sum_{i=1}^{k} \beta_i x_i + \sum_{i=1}^{k} \beta_{ij} x_i^2 + \sum_{i<j} \sum \beta_{ij} x_i x_j + \varepsilon \tag{7}$$

Table 6. Analysis of variance for aniline degradation (ANOVA Table)

Source	a) Before removing insignificant factors						b) After removing insignificant factors					
	DF	Seq SS	Adj SS	Adj MS	F	P-value	DF	Seq SS	Adj SS	Adj MS	F	P-value
Regression	14	792.24	792.24	56.59	44.32	0.000	12	791.92	791.92	65.99	59.09	0.000
Linear	4	198.72	198.72	49.68	38.91	0.000	4	198.72	198.72	49.68	44.49	0.000
Anil.	1	79.73	79.73	79.73	62.45	0.000	1	79.73	79.73	79.73	71.40	0.000
pH	1	54.36	54.36	54.36	42.57	0.000	1	54.36	54.36	54.36	48.68	0.000
H_2O_2	1	58.79	58.79	58.79	46.04	0.000	1	58.79	58.79	58.79	52.64	0.000
Cat.	1	5.84	5.84	5.84	4.57	0.054	1	5.84	5.84	5.84	5.23	0.038
Square	4	350.1	350.1	87.53	68.55	0.000	2	349.80	349.80	174.90	156.61	0.000
Anil. × Anil.	1	122.04	52.60	52.60	41.19	0.000	1	122.04	60.92	60.92	54.55	0.000
pH × pH	1	227.77	186.32	186.32	145.92	0.000	1	227.77	227.77	227.77	203.95	0.000
$H_2O_2 \times H_2O_2$	1	0.04	0.00	0.00	0.00	0.991	-	-	-	-	-	-
Cat. × Cat.	1	0.27	0.27	0.27	0.21	0.652	-	-	-	-	-	-
Interaction	6	243.39	243.39	40.57	31.77	0.000	6	243.39	243.39	40.57	36.32	0.000
Anil. × pH	1	16.00	16.00	16.00	12.53	0.004	1	16.00	16.00	16.00	14.33	0.002
Anil. × H_2O_2	1	73.78	73.78	73.78	57.78	0.000	1	73.78	73.78	73.78	66.07	0.000
Anil. × Cat.	1	78.79	78.79	78.79	61.71	0.000	1	78.79	78.79	78.79	70.55	0.000
pH × H_2O_2	1	57.12	57.12	57.12	44.73	0.000	1	57.12	57.12	57.12	51.15	0.000
pH × Cat.	1	6.09	6.09	6.09	4.77	0.050	1	6.09	6.09	6.08	5.45	0.035
H_2O_2 × Cat.	1	11.62	11.62	11.62	9.10	0.011	1	11.62	11.62	11.62	10.40	0.006
Residual error	12	15.32	15.32	1.28			14	15.64	15.64	1.12		
Lack-of-fit	10	13.58	13.58	1.36	1.55	0.454	12	13.89	13.89	1.16	1.32	0.509
Pure error	2	1.75	1.75	0.88			2	1.75	1.75	0.87		
Total	26	807.56					26	807.56				

Fig. 7. Degradation mechanism of aniline over MnFe₂O₄/Zn₂SiO₄ Nano photo-catalyst

$$\%Aniline\ degradation = 85.3716 + 2.58[Cat.] - 3.09[Aniline]^2 + 5.97[pH]^2 - 24.44[Aniline \times Cat.] + 3.78[pH \times H_2O_2][Aniline] + 2.13[pH] - 2.21[H_2O_2] + 0.7[Aniline \times pH] + 4.29[Aniline \times H_2O_2] + +1.23[pH \times Cat.] - 1.70[H_2O_2 \times Cat.]$$

(8)

Finally, response optimizer was applied to recognize the best operating conditions in order to optimize the aniline degradation, decrease cost, increase sensitivity of factors and desirability. Desirability values (D), according to optimization parameters, became equal to 0.913. Optimal factors for aniline, H_2O_2, pH and catalyst were determined equal to 5.5 ppm, 5.3 mM, 11 and 0.4 g/L, respectively. These factor settings are the best factor levels, which is called global solution. Also predicted value of the yield of aniline degradation became equal to 96%.

Table 7. Comparison of models

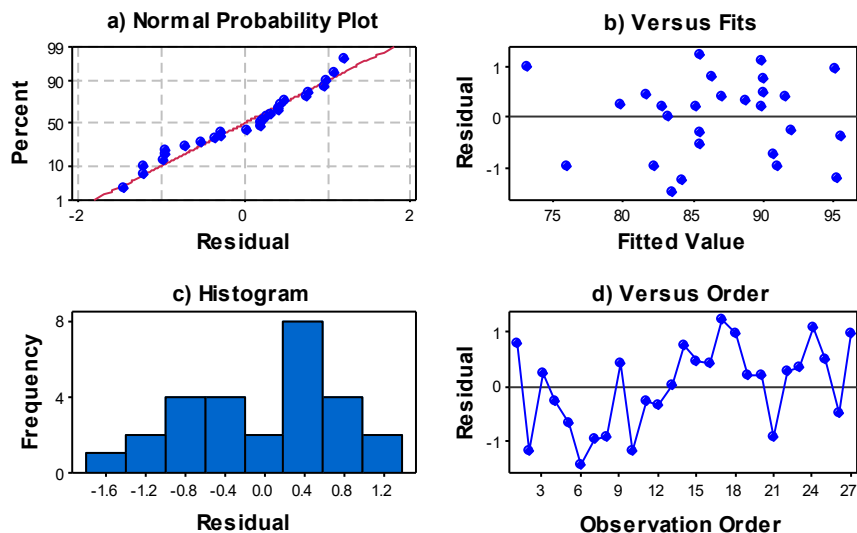| Model based on selected terms	Adj. R^2	P-value[a]	Suggestion
Linear	10.90 %	0.028	not adequate
Linear with squares	53.72 %	0.053	not adequate
Linear with interactions	26.47 %	0.033	not adequate
Full quadratic	96.40 %	0.509	suggested

Fig. 8. Residual plots for degradation: (a) Normal probability plot of residuals; (b) Residuals versus fitted values; (c) Histogram of the residuals; (d) Residuals versus order of data

Kinetics of photo-catalytic degradation of aniline

Fig. 9 displays the plot of Ln(A0/A) versus reaction time for aniline decomposition in optimum condition with different NPs. The linearity of the plot suggests that the photo-degradation reaction approximately follows the pseudo first order kinetics. The efficiency of $MnFe_2O_4$, Zn_2SiO_4 and $MnFe_2O_4/Zn_2SiO_4$ in relation to each other was compared in optimum conditions and the arrangement of ($MnFe_2O_4/Zn_2SiO_4$)> ($MnFe_2O_4$)> (Zn_2SiO_4) was obtained. The results of the kinetic experiments indicate that the activity of $MnFe_2O_4$ photo-catalyst has increased due to stability on the Zn_2SiO_4 as a base. The increase in the effective surface of the catalyst and the possibility of absorbing contaminants on the catalyst can be due to the increase of the activity.

In order to study the reproducibility of the efficiency of final photo-catalyst, all the depreciated NPs of $MnFe_2O_4/Zn_2SiO_4$ were collected, washed, dried and were reused for degradation of a new aniline solution to optimal conditions. This process was repeated five times continuously. Comparing the efficiency of degradation in each stage signifies that the activity of degradation nano photo-catalyst is considerably reproducible (Fig. 10).

CONCLUSION

In this research, $MnFe_2O_4$ supported on Zn_2SiO_4 was successfully produced via hydrolysis apply urea and co-precipitation method. Various techniques, such as XRD, XRF, FTIR, FESEM, EDXS, TEM and BET were employed to specify Characteristics of new $MnFe_2O_4/Zn_2SiO_4$ photo-catalyst. The results derived from of these techniques presented that the synthesized particles are in nano-scale and have a suitable surface area. The formation of the $MnFe_2O_4$ shell on the Zn_2SiO_4 core with a thickness of less than 15 nm was also confirmed. The efficiency of the $MnFe_2O_4/Zn_2SiO_4$ was corroborated through the photo-catalytic degradation process of aniline under simulated solar radiation; such efficiency is due to its nano-porous core–shell structure. The study revealed
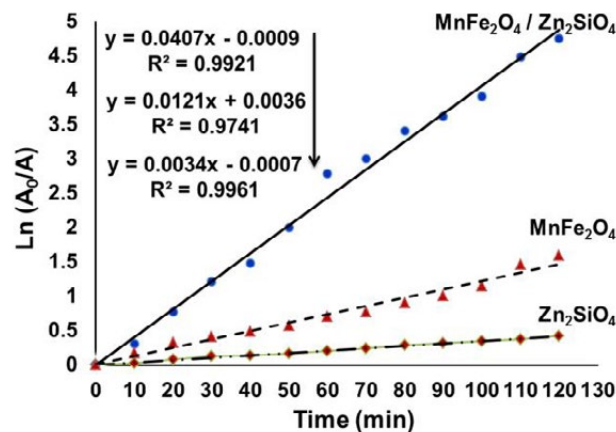
Fig. 9. Pseudo first order kinetics plot for photo-catalytic decomposition of aniline by (a) MnFe$_2$O$_4$; (b) Zn$_2$SiO$_4$; (c) MnFe$_2$O$_4$/Zn$_2$SiO$_4$ NPs

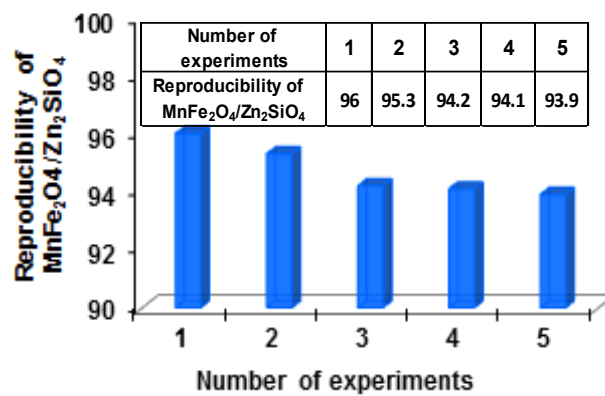| Number of experiments	1	2	3	4	5
Reproducibility of MnFe$_2$O$_4$/Zn$_2$SiO$_4$	96	95.3	94.2	94.1	93.9

Fig. 10. Reproducibility of MnFe$_2$O$_4$/Zn$_2$SiO$_4$

that DOE using RSM with Box-Behnken design approach is an excellent technic to specifying significant parameters, interaction factors and empirical model to optimize the aniline degradation, to decrease costs, to increase the sensitivity of factors and desirability. As presented, the statistical parameters such as adjusted R^2 (96.40%) and standard deviation of the residuals (1.05677) in full quadratic model affirmed the suitability of full quadric model in fitting the data. Moreover, the best operating conditions for factors of aniline, H$_2$O$_2$, catalyst and pH were obtained something equal to 5.5 ppm, 5.3 mM, 0.4 g L^{-1} and 11, respectively. Besides, the predicted value for photo-catalyst efficiency and desirability in aniline degradation also were achieved, equal to 96% and 0.913, in sequence. The efficiency of synthetic NPs in the following arrangement MnFe$_2$O$_4$/Zn$_2$SiO$_4$> MnFe$_2$O$_4$> Zn$_2$SiO$_4$ demonstrated the influence of base (Zn$_2$SiO$_4$) on activity of Mnfe$_2$O$_4$ due to the increase in the surface area of the photo-catalyst and the fast transfer of photoelectrons.

After five times comparing the efficiency of the depreciated photo-catalyst of MnFe$_2$O$_4$/Zn$_2$SiO$_4$ it indicated that the activity of nano photo-catalyst is considerably reusable, effective and efficient. Therefore, based on the evidence obtained, the development of studies and the use of MnFe$_2$O$_4$/Zn$_2$SiO$_4$ photo-catalyst in removal of other aromatic pollutants are recommended.

CONFLICT OF INTEREST

The authors declare that there are no conflicts of interest regarding the publication of this manuscript.

ABBREVIATIONS

Adj. MS	Adjusted mean squares
Adj. R^2	Adjusted R square
ANOVA	Analysis of variance
Adj SS	Adjusted sum of squares
AOP	Through the advanced oxidation process
BET	Brunauer–Emmett–Teller
BJH	Barclay James Harvest
Deg%	Percentage of aniline degradation
D	Desirability value
DF	Degree of freedom
DOE	Design of experiment
EDXS	Energy-dispersive X-ray spectroscopy
FESEM	Field emission scanning electron microscopy
FTIR	Fourier-transform infrared spectroscopy
F	F-value
MRI	Magnetic resonance imaging
MWCNT	Multi-walled carbon nanotubes
NPs	Nano particles
PRESS	Prediction error
Pred. R^2	Predicted R square
P	P-values (probability value)
RSD	Response surface design
RSM	Response surface methodology
PSO	Pseudo first order
R^2	R square
Seq. SS	Sequential sum of squares
S	Standard deviation of the residuals
UV-Vis	Ultraviolet–visible
XRD	X-ray diffraction
XRF	X-ray fluorescence
Y	Aniline degradation yield (Response)

REFERENCES

1. Wei Z, Faul CFJ. Aniline Oligomers – Architecture, Function and New Opportunities for Nanostructured Materials. Macromolecular Rapid Communications. 2008;29(4):280-92.

2. Al-Nu'airat J, Altarawneh M, Gao X, Westmoreland PR, Dlugogorski BZ. Reaction of Aniline with Singlet Oxygen (O2 1Δg). The Journal of Physical Chemistry A. 2017;121(17):3199-206.

3. Fakhru'l-Razi A, Pendashteh A, Abdullah LC, Biak DRA, Madaeni SS, Abidin ZZ. Review of technologies for oil and gas produced water treatment. Journal of Hazardous Materials. 2009;170(2-3):530-51.

4. Chong MN, Jin B, Chow CWK, Saint C. Recent developments in photocatalytic water treatment technology: A review. Water Research. 2010;44(10):2997-3027.

5. Kamble SP, Sawant SB, Schouten JC, Pangarkar VG. Photocatalytic and photochemical degradation of aniline using concentrated solar radiation. Journal of Chemical Technology & Biotechnology. 2003;78(8):865-72.

6. Tang H, Li J, Bie Y, Zhu L, Zou J. Photochemical removal of aniline in aqueous solutions: Switching from photocatalytic degradation to photo-enhanced polymerization recovery. Journal of Hazardous Materials. 2010;175(1-3):977-84.

7. Anotai J, Jevprasesphant A, Lin Y-M, Lu M-C. Oxidation of aniline by titanium dioxide activated with visible light. Separation and Purification Technology. 2012;84:132-7.

8. Pirsaheb M, Shahmoradi B, Beikmohammadi M, Azizi E, Hossini H, Md Ashraf G. Photocatalytic degradation of Aniline from aqueous solutions under sunlight illumination using immobilized Cr:ZnO nanoparticles. Scientific Reports. 2017;7(1).

9. Norzaee S, Djahed B, Khaksefidi R, Mostafapour FK. Photocatalytic degradation of aniline in water using CuO nanoparticles. Journal of Water Supply: Research and Technology - Aqua. 2017;66(3):178-85.

10. Talebian N, Jafarinezhad F. Morphology-controlled synthesis of SnO2 nanostructures using hydrothermal method and their photocatalytic applications. Ceramics International. 2013;39(7):8311-7.

11. Kumar A, Mathur N. Photocatalytic degradation of aniline at the interface of TiO2 suspensions containing carbonate ions. Journal of Colloid and Interface Science. 2006;300(1):244-52.

12. Orge CA, Faria JL, Pereira MFR. Photocatalytic ozonation of aniline with TiO 2 -carbon composite materials. Journal of Environmental Management. 2017;195:208-15.

13. Das I, Ansari SA. Nanomaterials in Science and Technology. 2009; 68: 657-667.

14. Taffa DH, Dillert R, Ulpe AC, Bauerfeind KCL, Bredow T, Bahnemann DW, et al. Photoelectrochemical and theoretical investigations of spinel type ferrites (MxFe3–xO4) for water splitting: a mini-review. Journal of Photonics for Energy. 2016;7(1):012009.

15. Faraji M, Yamini Y, Rezaee M. Magnetic nanoparticles: Synthesis, stabilization, functionalization, characterization, and applications. Journal of the Iranian Chemical Society. 2010;7(1):1-37.

16. Zhao L, Deng J, Sun P, Liu J, Ji Y, Nakada N, et al. Nanomaterials for treating emerging contaminants in water by adsorption and photocatalysis: Systematic review and bibliometric analysis. Science of The Total Environment. 2018;627:1253-63.

17. Takesue M, Hayashi H, Smith RL. Thermal and chemical methods for producing zinc silicate (willemite): A review. Progress in Crystal Growth and Characterization of Materials. 2009;55(3-4):98-124.

18. Myers RH, Montgomery DC. Response surface methodology: process and product optimization using designed experiments: Wiley New York; 1995.

19. Amighian J, Mozaffari M, Nasr B. Preparation of nano-sized manganese ferrite (MnFe2O4) via coprecipitation method. physica status solidi (c). 2006;3(9):3188-92.

20. Bharathi S, Nataraj D, Mangalaraj D, Masuda Y, Senthil K, Yong K. Highly mesoporous α-Fe2O3nanostructures: preparation, characterization and improved photocatalytic performance towards Rhodamine B (RhB). Journal of Physics D: Applied Physics. 2009;43(1):015501.

21. Sam S, Nesaraj AS. Preparation of MnFe2O4 nano-ceramic particles by soft chemical routes. Int J Appl Sci Eng. 2011;9(4):223-239.

22. Zhang S, Lu M, Li Y, Sun F, Yang J, Wang S. Synthesis and electrochemical properties of Zn2SiO4 nano/mesorods. Materials Letters. 2013;100:89-92.

23. Lukić S, Petrović D, Đačanin L, Marinović-Cincović M, Antić Ž, Krsmanović R, et al. Gel combustion synthesis

of transition metal ions doped Zn2SiO4 powder. Journal of Optoelectronics and Advanced Materials. 2008;10(10):2748-2752.

24. Alibe I, Matori K, Sidek H, Yaakob Y, Rashid U, Alibe A, et al. Effects of Calcination Holding Time on Properties of Wide Band Gap Willemite Semiconductor Nanoparticles by the Polymer Thermal Treatment Method. Molecules. 2018;23(4):873.

25. kanagesan S, Aziz S, Hashim M, Ismail I, Tamilselvan S, Alitheen N, et al. Synthesis, Characterization and in Vitro Evaluation of Manganese Ferrite (MnFe2O4) Nanoparticles for Their Biocompatibility with Murine Breast Cancer Cells (4T1). Molecules. 2016;21(3):312.

26. Wang W, Ding Z, Cai M, Jian H, Zeng Z, Li F, et al. Synthesis and high-efficiency methylene blue adsorption of magnetic PAA/MnFe2O4 nanocomposites. Applied Surface Science. 2015;346:348-53.

27. Zipare K, Dhumal J, Bandgar S, Mathe V, Shahane G. Super-paramagnetic manganese ferrite nanoparticles: synthesis and magnetic properties. Journal of Nano-science and Nano-engineering. 2015;1(3):178-182.

28. Thommes M, Kaneko K, Neimark AV, Olivier JP, Rodriguez-Reinoso F, Rouquerol J, et al. Physisorption of gases, with special reference to the evaluation of surface area and pore size distribution (IUPAC Technical Report). Pure and Applied Chemistry. 2015;87(9-10):1051-69.